Investigating the Earth's upper mantle structure: numerical and laboratory experiments on mantle flow and entrainment processes

[1]Hamburg University
Inst. of Geophysics

J. Hasenclever[1], J. Phipps Morgan[2] and M. Hort[1]

[2]Cornell University
Earth and Atmospheric Sciences

Introduction

We investigate the geodynamical implications of a relative low density and low viscosity asthenosphere layer sandwiched between overlying strong oceanic lithosphere (>10^{25} Pa s) and underlying more viscous (~10^{21} Pa s) mantle material. Several studies support the existence of a weak (10^{18-19} Pa s) layer in the uppermost oceanic mantle, e.g. seismic observations of radial Earth structure, studies on the distribution of stresses in oceanic plates, and post-glacial rebound modeling (see Phipps Morgan et al., JGR 100, pp.12753, 1995, for a short review).

In the scenario explored the asthenosphere originates from upwelling mantle plumes that melt to a few degrees beneath hotspots to form OIBs. The depleted residual material (96-99% of the mass upwelled in plumes) ponds underneath the lithosphere and forms a hot, thus buoyant and weak asthenosphere layer. As the asthenosphere rises underneath mid-ocean ridges a second melting process forms depleted MORB but roughly 85% of the original plume mass remains as an extremely depleted layer. The above processes are part of the "plum-pudding" Earth-model proposed by Phipps Morgan and Morgan, (EPSL 170, pp.215, 1999).

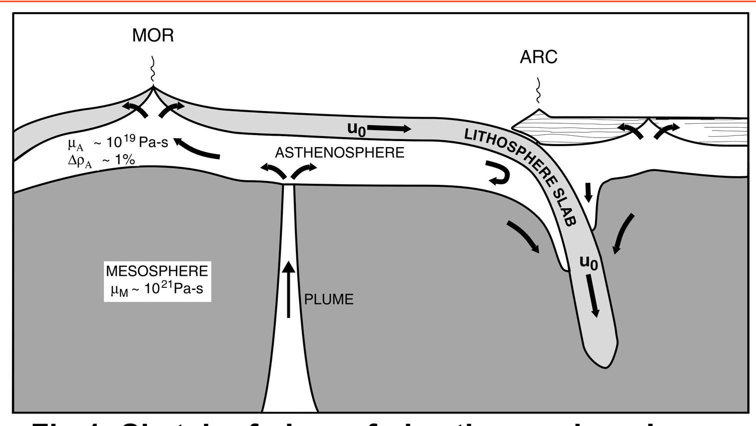

Fig 1: Sketch of plume-fed asthenosphere layer

In detail we address the following questions:
- How is flow within the upper mantle affected by the presence of a weak and buoyant asthenosphere layer?
- Is most of the buoyant upper asthenosphere removed at subduction zones or is it conserved so that a weak and buoyant layer could establish during the Earth's history?

The numerical model

We're using a two-dimensional numerical model that combines finite element and finite difference techniques to solve for viscous flow and temperature, respectively. A tracer particle advection scheme is used to watch asthenosphere propagation which helps limit numerical diffusion at compositional boundaries (i.e. at asthenosphere boundaries). Each tracer particle represents a small volume of asthenosphere. Asthenosphere properties (Fe-depletion buoyancy and elevated temperature) are mapped onto the grid points and affect viscosity and consequently the flow field. Density variations due to thermal and compositional changes are considered in the buoyancy term only (Boussinesq approximation). The weighted numerical grid has an increased resolution of up to 4km in the slab surroundings. Melting processes, thus compositional changes during a numerical calculation are not included.

The oceanic and overriding plate side of the slab are simulated separately in closed rectangular boxes. Slab and lithosphere are implemented as velocity and temperature boundary conditions; top boundaries are insulating representing the base of overlying lithosphere, heat conduction occurs into the slab moving at a fixed 45° angle of subduction. The initial 200 km thick asthenosphere layer is prescribed to be up to 1% less dense than underlying mantle. Asthenosphere viscosity, subduction rate, and slab age varied in a suite of experiments.

Results of numerical modeling

The typical mantle flow field exhibited in our experiments is shown in **Fig 2**, which represents an inset near the slab, combining the results for separately conducted numerical experiments for each side of the slab.

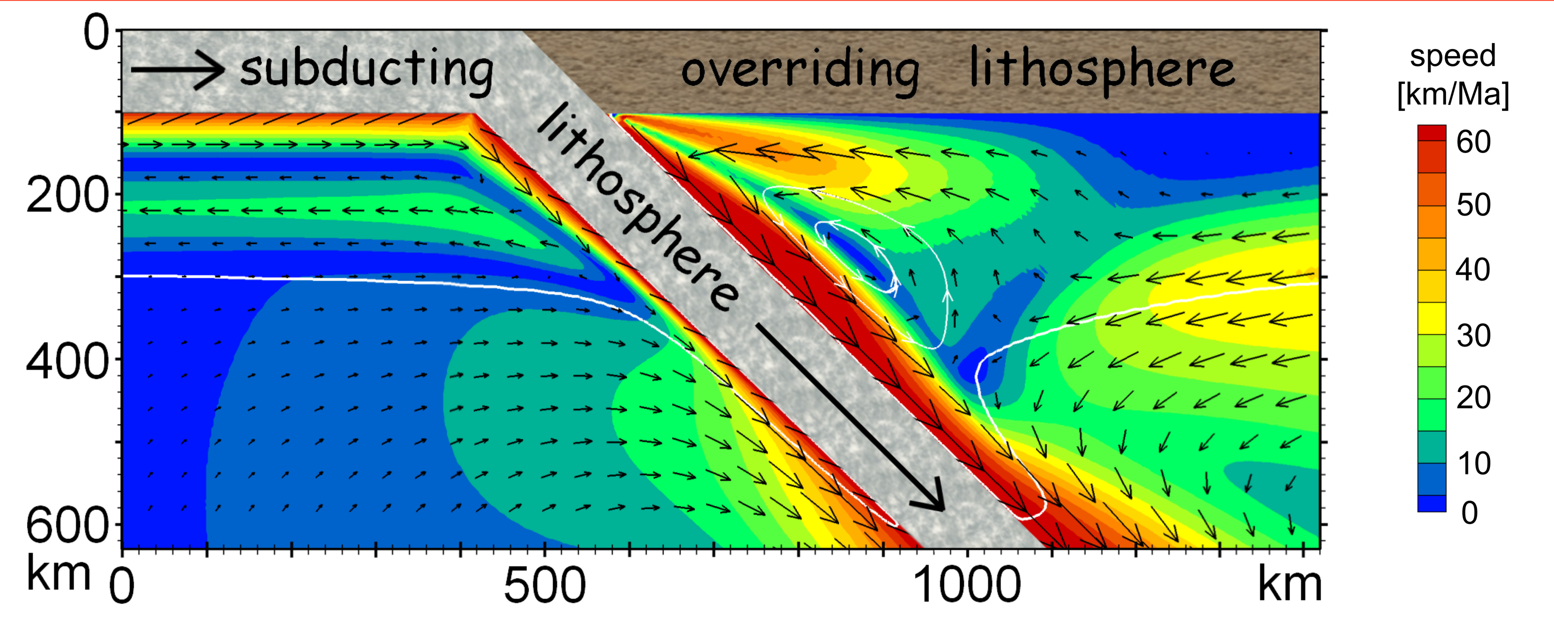

Fig 2: Mantle flow and asthenosphere entrainment at a subduction zone.
White lines encompass asthenospheric material, arrows show flow directions, and colors are flow speeds. Low viscosity/low density asthenospheric material is entrained on the hot bottom side of the slab by downdrag only, with thicknesses of the entraining finger ranging from 10 km to 55 km (**Fig 3a**). At the cold top of the slab, entrainment is much larger for the same model parameters with about twice the entrainment thickness subducting (**Fig 3b**), roughly half by cooling and 'freezing' to the top of the slab and half by downdragging like at the slab's base. Beneath the oceanic lithosphere a return flow towards the mid-ocean ridge develops while a recirculation forms in the mantle wedge (white streamlines).

At the slab's bottom-side asthenosphere entrains by downdragging only, the rate depends upon the asthenosphere viscosity and the subduction rate (**Fig 3a**). Conductive heat loss into the colder top of the slab and the consequent viscosity increase result in higher rates on this side (**Fig 3b**) – here older oceanic lithosphere entrains more asthenosphere than younger plates due to the steeper temperature gradient in older slabs.

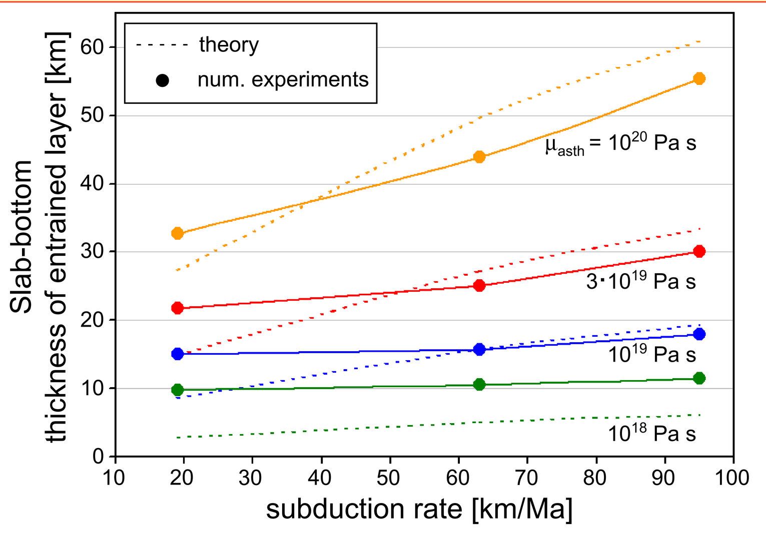

Fig 3a: Asthenosphere entrainment at slab's bottom. Solid lines show results based on numerical calculations (solid circles). Dashed lines are theoretical maximum entrainment rates derived from a boundary layer theory (see right-hand side of the poster).

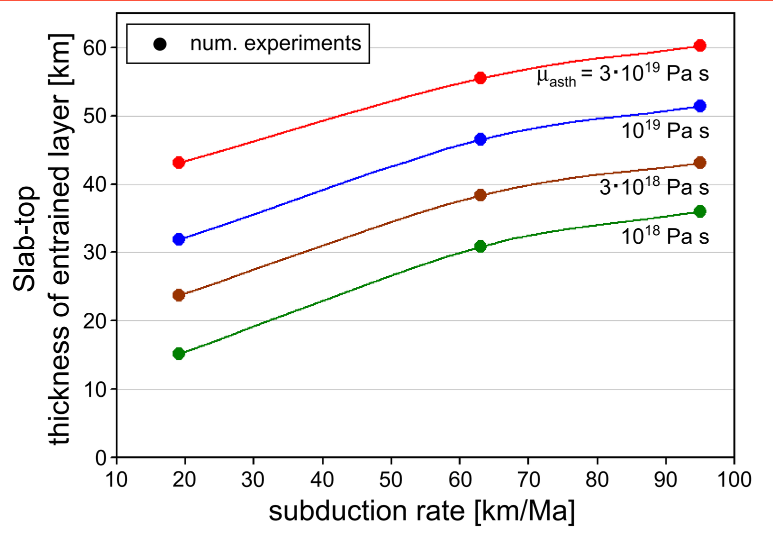

Fig 3b: Asthenosphere entrainment at slab's top. Solid lines show results based on numerical calculations (solid circles). For same model parameters entrainment rates are roughly twice as high as for the bottom side.

Dashed lines in **Fig 3a** are based on a boundary layer theory (see right-hand side of the poster) and are in good agreement with the numerical results for the moderate to large asthenosphere viscosities (10^{19} up to 10^{20} Pa-s) which are numerically best resolved. Possibly the growing relative importance of conductive heat loss with decreasing subduction speed is the main reason for the more strongly deviating numerical results at the lowest subduction rates. For the lowest asthenosphere viscosity considered, the boundary layer theory consistently predicts smaller entrainment thicknesses than observed in the numerical calculations, which we think is predominantly an effect of poor numerical resolution of the thin entrainment boundary layer.

Code verification (1) laboratory experiments

Experiments are conducted in a Plexiglas reservoir of 50x30x10cm size filled with two unequal layers of syrup (**Fig 4**). Viscosity and density of the syrup are varied by adding water. A plastic film is pulled on top of the syrup and along an inclined plate to initiate the motion of the oceanic lithosphere. The driving mechanism consists of an electric motor and a reduction gear unit that allows for 'plate' speeds ranging from 0.5 to up to 5 cm/min. A vertical center cross-section is lit up through a slot so that glass beads in the upper layer reflect the light and show the syrup's motion and the interface between the layers.

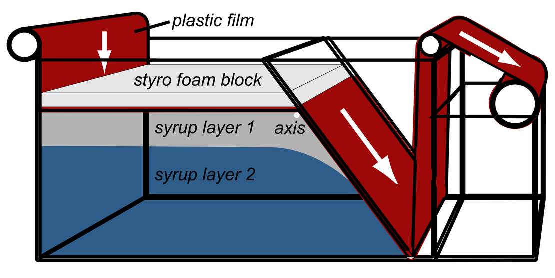

Fig 4: Setup of lab experiments

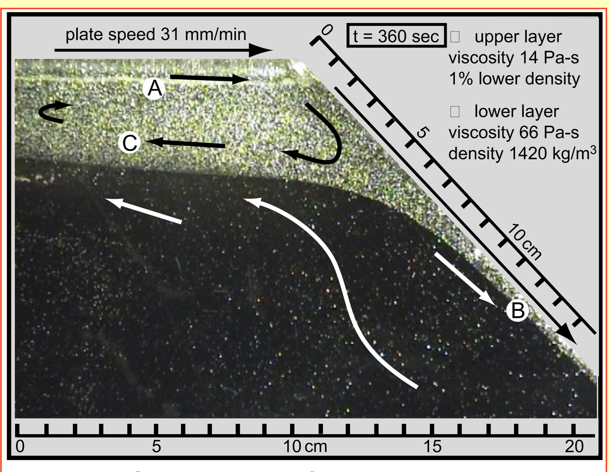

Fig 5: Snap-shot of a lab experiment

Fig 5 is a snap-shot of a video recording showing a section of the reservoir during a relatively fast subduction experiment. The uppermost low-viscous syrup is dragged towards the right side (A). Along the inclined right boundary a small portion is entrained (B), whereas most of the upper syrup feeds a return flow towards the left side (C). The interface between the two layers is tilted towards the right side because viscous resistance to the return flow causes a pressure high beneath the trench.

A numerical simulation of the above laboratory experiment is shown in **Fig 6.** The syrup viscosities and densities as well as tank dimensions are considered. Similar results for interface tilt, thickness of entrained finger and the flow field are observed. The return flow within the upper layer and the much weaker flow in the lower layer show similar speeds and directions in both numerical and laboratory experiments.

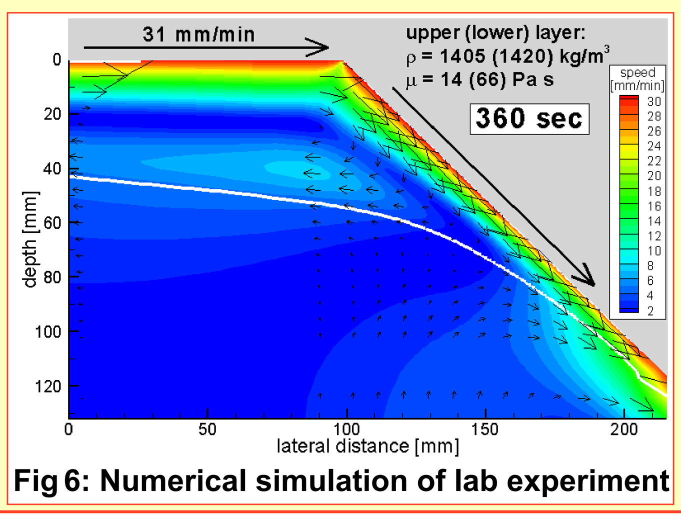

Fig 6: Numerical simulation of lab experiment

Code verification (2) analytical solutions

A boundary layer theory was developed to estimate the entrainment beneath the base of the subducting slab. We treat the entrainment process as the Poiseuille flow problem sketched in **Fig 7** neglecting the conductive heat loss into the slab. The slab and adjacent mantle drag down a finger of buoyant asthenosphere at a flux $Q_{down} = u_0$ h, where u_0 is the speed of the slab and h the thickness of the entraining finger. Within the finger itself, local buoyancy resists subduction resulting in an upward flux $Q_{up} = (h^3/12\mu_A)\ \Delta\rho\ g$.

The net flux is the difference of the two opposing flux components:

$$Q_{net} = Q_{down} - Q_{up} = u_0\ h - (h^3/12\mu_A)\ \Delta\rho\ g$$

Maximum entrainment as a function of h occurs at

$$dQ_{net}/dh = 0 = u_0 - (h^2/4\mu_A)\Delta\rho g.$$

The thickness of the entraining finger for maximum entrainment is

$$h_E = (4\mu_A u_0/\Delta\rho g)^{-1/2}$$

which is used to verify those observed in the numerical experiments.

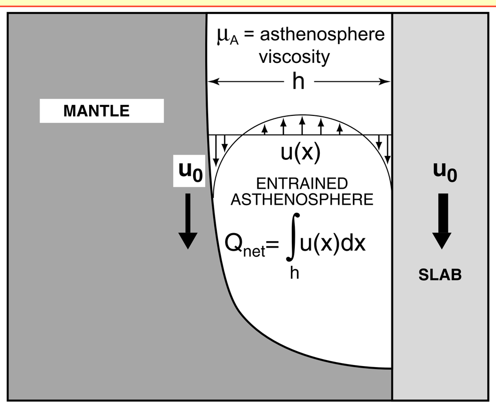

Fig 7: Boundary layer theory for asthenosphere entrainment

The analytically derived finger thicknesses at maximum entrainment rate are compared to those found in the numerical simulations for the slab's bottom side (**Fig 8**). The numerical results show higher values than theoretically expected if a too coarse numerical grid is used. On top of the slab the entrainment rates are much higher than those underneath the slab due to the additional freezing effect. Here an analytical solution is hard to find and numerical calculations are necessary.

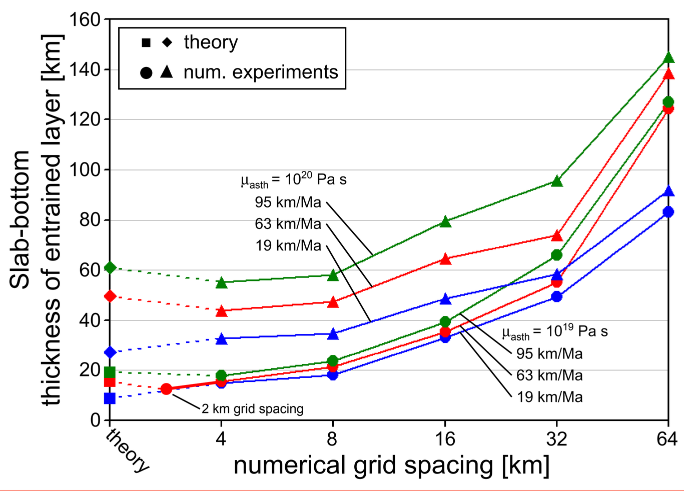

Fig 8: Thickness of the entrained asthenosphere finger as observed in numerical experiments using different numerical grid-spacing. Numerical results for two asthenosphere viscosities and three subduction rates are shown. The respective theoretical maximum thickness is marked at the 'zero' grid-size edge of the plot. Artificially high asthenosphere entrainment is observed until a fine mesh of ~4km is used to model flow in the region of the entrained finger. Very time consuming calculations on a fine numerical grid deliver entrainment rates that are lower than the maximum. This implies that the analytical approach discussed above is valid and that numerical resolution (i.e. the grid-spacing) has a main impact on the results of numerical simulations.

Implications for mantle flow and mantle evolution

Numerical models, in accord with laboratory experiments and boundary layer theory, show limited entrainment at subduction zones. If a buoyant low viscosity asthenosphere layer forms, the subduction entrainment is an inefficient way to bring it back into the deeper mantle – instead asthenosphere is mainly 'consumed' by accreting into cold lithosphere and subducting as a slab.

Entrainment is likely to be greater on the arc-side of the slab than on the seaward side, since the much stronger temperature gradient at the top-face of the slab causes freezing of adjacent asthenosphere.

Back-arc recirculation can easily develop in the mantle wedge as a 'corner flow' solution does not exist when the asthenosphere is more buoyant than underlying mantle. This may have important implications for the time-evolution of arc magmatism and back-arc extension.

None of the effects observed (limited entrainment, return flow, recirculation) will be resolvable in global 3-D mantle convection codes until they can incorporate a ~5-10 km numerical resolution of low viscosity regions adjacent to higher viscosity subducting slabs – if a numerical experiment's resolution is lower than this, it will tend to improperly entrain too much asthenosphere as an artifact.

Current work and Outlook

Current work focuses on the implications of a plume-fed asthenosphere layer for mantle flow and melting processes at mid-ocean ridges and for plume-ridge interaction. For this purpose the tracer advection scheme has been modified in that **each tracer is now able to track multiple pieces of geophysical and geochemical information**, for example its degree of melting. Each tracer reacts individually to the temperature and pressure conditions it passes through and, in turn, affects these grid-specific variables. For example, temperature is calculated for a tracer's position and the melting rate of the tracer is mapped onto the grid where it affects the temperature field due to latent heat loss.

Since the number of variables that can be stored in each tracer is only limited by the computer's memory, this method can simultaneously track more than one mantle component, for example a depleted and an enriched component that melt at different depths and at different rates. Representative trace element contents and isotope ratios for each mantle component are also stored with the moving tracers particles, so that the geochemical evolution of a small mantle volume is recorded in each tracer. The tracer method and some preliminary results are presented below.

Current work: Interaction of mantle flow and melting at mid-ocean ridges Incorporation of geochemistry in a mantle flow model

During the last decades, flow and melting processes at mid-ocean ridges have been investigated by various authors focussing on either the solid mantle flow (e.g. the effects of transform faults, ridge migration or plume-ridge interaction) or the geochemistry of MORB. We are developing a numerical model for solid mantle flow that can incorporate different mantle components as sources for melt generation by using a modified tracer particle advection scheme. Either a tracer particle can be made up of a single component to 100vol% (i.e. there are tracers representing a depleted mantle component and some representing an enriched component) or each tracer contains several mantle components (e.g. each tracer begins with 80vol% depleted and 20% enriched mantle). In this way mantle heterogeneities of various sizes can be considered, ranging from mantle plume-size (using "plume"- and "upper mantle"-tracers) down to small volumes that are always in thermal equilibrium (many components in one tracer).

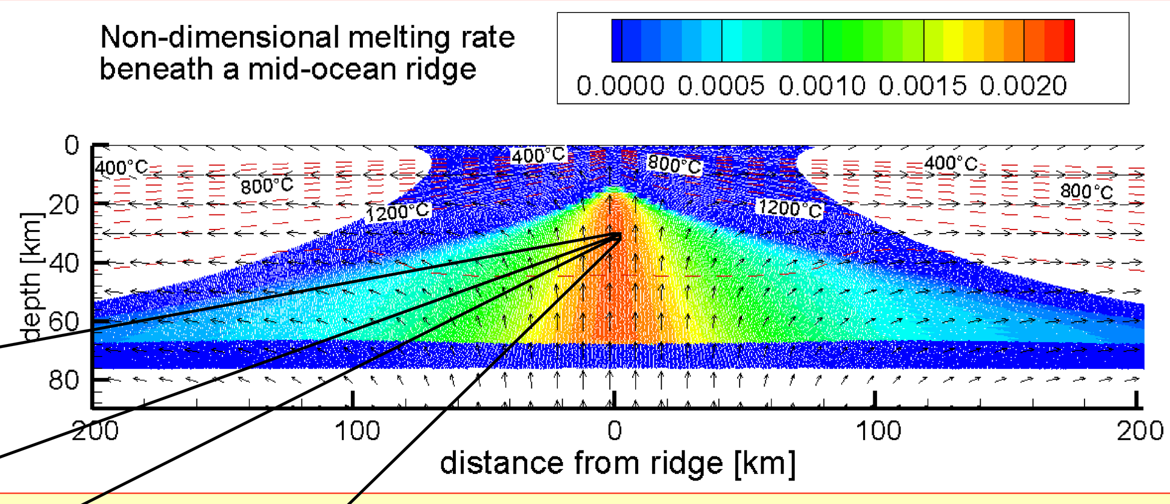

Fig 9: Two-dimensional model calculation of mid-ocean ridge melting. "Intelligent" tracer particles are advected in an analytical corner flow solution and melt according to their depth and temperature. Vectors show the flow field, red dahed lines are isotherms. White regions are free of tracers that are initialized dynamically at 75 km depth.

Fig 10: Zooming into the melting zone...
Tracers are randomly displaced during initialization. Vectors show direction of advection, melting rates (colors) and isotherms (red dashed lines) are more detailed compared to **Fig 9**. Thin solid lines mark the numerical grid cells – the tracer method runs stably even for few (<5) tracers within one grid cell.

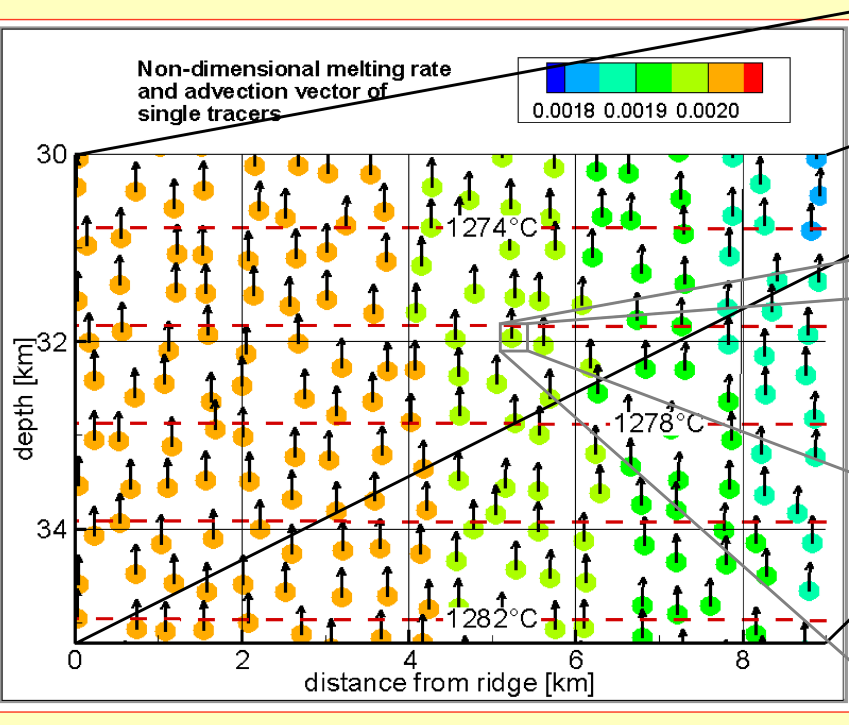

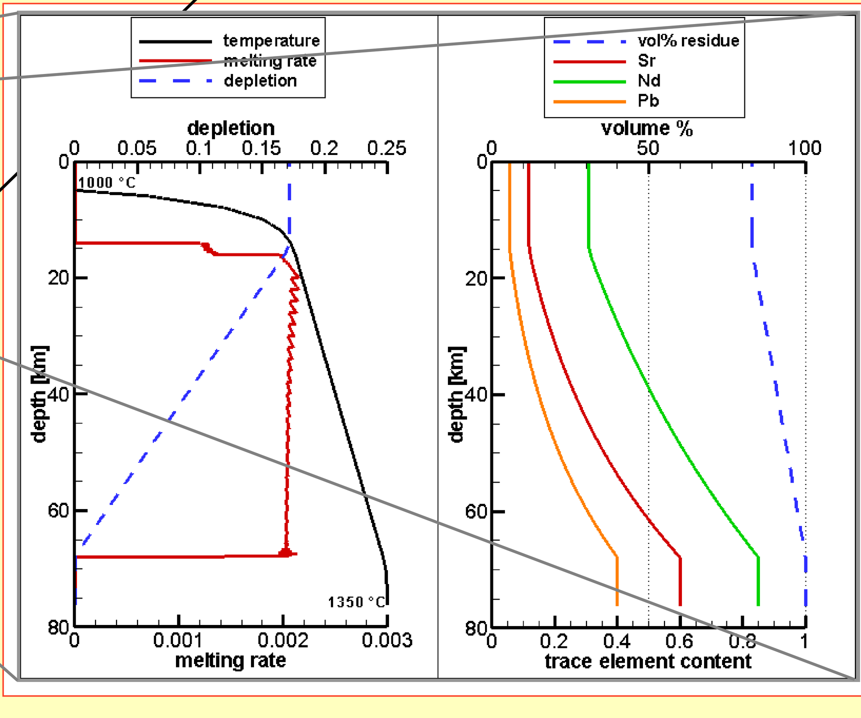

Fig 11: Record of a single tracer. Each tracer records its melting rate which is a function of the tracer's depth and the interpolated temperature at the tracer's position. Based on this melting rate the tracer partially melts, reduces its volume, and loses trace elements to the melt (which is instantaneously removed in the current version). These recordings allow the calculation of the melt composition at specific depths or distances from the ridge.

Each mantle component is characterized by a unique solidus function and specific trace element contents and isotope ratios. During a numerical calculation the geochemical properties of small mantle volumes evolve in response to the T-p conditions the tracer particles pass through. Outcomes of test-runs using a steady state cornerflow solution (**Fig 9**) are the trace element contents as a function of depth (**Fig 11**). During a model calculation tracers are dynamically initialized beneath the melting zone and removed as they leave the melting zone at some distance from the ridge-axis. Data from removed tracers is used to calculate the residual melting column.